

## NUMERICAL VALIDATION OF THE HYDRODYNAMIC DRAG OF A SURFACED AND FULLY APPENDED UNDERWATER VEHICLE

Reference NO. IJME716, DOI No: 10.5750/ijme.v164i1.24

**M Courdier**, Australian Maritime College, Australia, **Z Leong**, Australian Maritime College, Australia, **J Duffy**, Australian Maritime College, Australia, **J Binns**, Australian Maritime College, Australia, **A Conway**, Defence Science and Technology Group, Australia

KEY DATES: Submitted: 07/04/22; Final acceptance: 22/04/22; Published 15/06/22

### SUMMARY

Underwater Vehicles (UV) are required to travel on the surface for periods of time to complete mission requirements. However, knowledge on the drag of a surfaced UV is scarce in the public domain and the knowledge on the behaviour of surface craft is generally not applicable due to substantial differences in hull form. This paper presents a numerical study on the drag coefficient of a surfaced and fully appended BB2 UV in calm water. The results were firstly validated with the available experimental drag data for a range of speeds. Secondly, the free surface elevation along the length of the UV photographed during physical model scale experiments is compared to the free surface elevation predicted by CFD. This research has shown that a multiphase CFD model can accurately predict the drag due to the forward motion of a surfaced UV in calm water.

### NOMENCLATURE

ACS	Aft Control Surfaces
AMC	Australian Maritime College
BOI	Body of Influence
Cd	Drag Coefficient
CFD	Computational Fluid Dynamics
D	Diameter (m)
DST	Defence, Science & Technology Group
Fr	Length Froude number (-)
$L_{pp}$	Length between perpendiculars (m)
LVDT	Linear Variable Differential Transformer
Re	Reynolds number (-)
U	Velocity of body centre of buoyancy relative to fluid ( $m\ s^{-1}$ )
UV	Underwater Vehicle
$W_s$	Wetted Surface area ( $m^2$ )
X	Drag force (N)
$X'$	Drag force coefficient (-); $X/(0.5\rho U^2 L^2)$
xCB	Centre of buoyancy from bow (m)
y+	Non-dimensional wall distance; $(u*y_{wall})/\nu$
x,y,z	Cartesian coordinates in the x,y,z-direction (m)
$\rho$	Fluid density ( $kg\ m^{-3}$ )
$\mu$	Fluid dynamic viscosity ( $kg\ m^{-1}\ s^{-1}$ )
$\nu$	Fluid kinematic viscosity ( $m^2\ s^{-1}$ ); $\mu/\rho$
$\nabla$	Hull Volume ( $m^3$ )

### 1. INTRODUCTION

Underwater Vehicles (UV) range in application from military operations to the collection of scientific data or industrial surveys (Alvarez et al., 2009; Renilson, 2018). These applications are typically performed at a depth considerably greater than the length of the vehicle. As such, data on the operation of an UV under the influence of the free surface is scarce in the public domain as studies have been predominantly performed for operations at depth (Gates and Lynn, 1990; Bovis, 2017; Renilson, 2018). The present research focusses on a surfaced UV as the wide majority need to operate at (or near) the surface for considerable periods of time whether to communicate, to (re)orientate themselves, to recharge batteries or air supplies, or to join a naval base or mother ship. To better understand the hydrodynamic conditions UVs are facing during their prolonged surfaced intervals, drag and wave-making characteristics thus need to be considered for evolutions in this environment.

The hydrodynamic characteristics of a surfaced UV are very different to its submerged condition. While seakeeping behaviour of a surface vessel has been widely studied, with a good level of understanding to support its design and operation (Lewis, 1988b), recent studies on the surfaced BB2 generic submarine by Blackman (2019) and McLean (2019) have shown that UVs have some distinct differences regarding their added resistance. This is also the case regarding their motions and seakeeping behaviour and will be the focus of a later study. The assumption that general surface ship knowledge would be widely applicable is hence inappropriate. For instance, it is well known that the drag of a surface ship generally increases with its speed (Alvarez et al., 2009; Doutreleau, Laurens and Jodet, 2011) and it is also generally accepted that an increase in wave height is responsible for greater

opposition to the forward motion, i.e. the larger the wave height, the greater the drag (Lewis, 1988b). However, McLean (2019) found that submarines experience a negative added resistance in waves at low encounter frequencies (non-dimensional frequency  $<2.0$ ), meaning that there is an energy gain from the hull's perspective. Blackman (2019) and McLean (2019) also showed that the total added drag decreased at higher forward speeds. This has also been confirmed by Daum et al. (2017) in the case of near surface submarines and contradicts the results of conventional surface vessel behaviour (Rameswar. Bhattacharyya, 1978). More generally it has been shown that the speed has a significant influence on the seakeeping behaviour (heave and trim motion responses in particular) of surfaced UVs (Hermanski and Kim, 2010; Blackman, 2019), for which particulars heave and trim coupling are observed. Previous research has also shown that some Small-Waterplane Area Twin Hull vessels exhibit a similar negative added resistance at low encounter frequencies, but research on causes remains fragmented (Chun, 1992).

The previous points support that a surfaced UV does not react the same way as conventional surface ships, and that little information on the behaviour of a surfaced UV is available in the public domain. Of particular interest is the drag and the body's motion response to waves, as these two criteria affect both the operational capabilities and the mission profile of a surfaced UV.

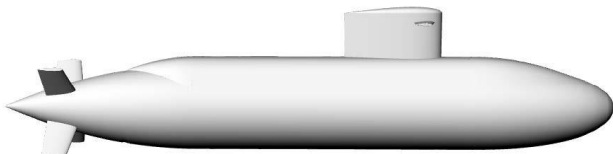


Figure 1: Fully appended BB2 generic hull geometry

This paper presents findings from a numerical study on the drag of a surfaced and fully appended BB2 generic hull (see Figure 1) in straight-line over a range of constant speeds in calm water. The Computational Fluid Dynamics (CFD) model utilised the Shear Stress Transport (SST) specific model coupled with the  $k-\omega$  turbulence model and a second order spatial discretization as it has been proven to provide accurate results that are comparable with experimental values for recovering the hydrodynamics coefficients of a submerged UV with low drift and pitch angle motions and within reasonable computation timeframe (Leong et al., 2015; Huong, 2018). The same model has been used for the surfaced conditions in this study as no notable differences were foreseen in its applicability. The free surface was modelled using a Volume of Fluid (VoF) method. Simulations were performed with the commercial CFD code ANSYS Fluent in steady state. This paper presents the comparison between numerical results for one degree of freedom (surge) and measurements from physical scale model towing tank tests. Good correlation is observed for the drag force,

as well as good comparison between the numerically predicted free surface elevation along the UV and the free surface elevation photographed during the physical model experiments. Hence, validating the CFD model.

The authors anticipate the developed CFD methodology presented in this paper to be a starting point for further in-depth studies of the seakeeping response of a surfaced UV hull in calm water and in waves with three degrees of freedom and overset meshes.

## 2. MODEL GEOMETRY AND SIMULATION SETUP

### 2.1 CHARACTERISTICS OF THE BB2 MODEL

A fully appended BB2 model is used in this study, as defined by Overpelt et al. (2015), and the numerical model presented an accuracy of 0.001m compared to the theoretical geometric shapes giving a satisfactory model representation. This model was selected as it represents a modern conventionally powered submarine, and experimental validation data were previously acquired in the research program developed at the Australian Maritime College (AMC) through a DST/AMC collaborative research project (Blackman, 2019; McLean, 2019). Experiments were performed with an artificial flow tripping device, in the form of a Hama Strip of 0.5 mm thick, located on the hull at 5%  $L_{pp}$  from the nose as per Kumar et al. (2018). Table 1 presents the major geometric characteristics of the model presented in Figure 2. The length between perpendiculars was used as the characteristic length for all the non-dimensionalisations presented in this study. A body-fixed reference frame was used with a positive x-axis towards the hull's bow and a positive z-axis upwards. The origin O of the frame was positioned on the hull Centre of Buoyancy (CB).

Table 1: Geometric characteristics of the BB2 model

Description	Symbol	Value	Unit
Length between perpendiculars	$L_{pp}$	1.692	[m]
Mid body diameter	$D$	0.231	[m]
Wetted surface area	$W_s$	0.822	[m <sup>2</sup> ]
Hull volume	$V$	0.051	[m <sup>3</sup> ]
Centre of buoyancy (from bow)	$x_{CB}$	0.914	[m]
Midship draft	$T_{MS}$	0.198	[m]

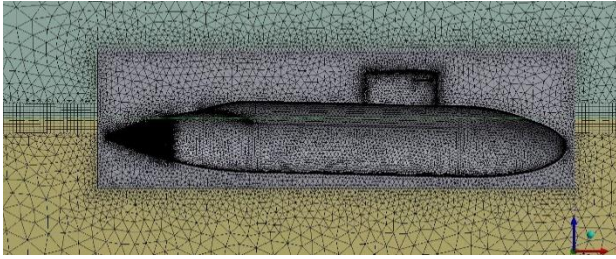


Figure 2: Mesh model overview of the BB2 geometry used for the tests at Length Froude number (Fr) 0.273, with inflation layers around free surface and mesh body of influence around the hull visible. The model is set at 1.577 degrees trim to match the experiment condition.

## 2.2 CHARACTERISTICS OF THE DOMAIN

The dimensions and test conditions for the CFD domain were modelled the same as in the AMC Towing Tank to enable direct comparison to the experimental data, as presented in Table 2. However, the inlet and outlet surfaces were positioned  $3xL_{pp}$  forward and  $5xL_{pp}$  aft from hull bow and stern respectively, in accordance with guidelines (ITTC, 2011), for a total domain length of 15.228m. For a similar purpose of computing time reduction, only half the domain was modelled using a XZ symmetry plane passing through the hull centre of buoyancy, and  $2/3$  of the water depth was used as air clearance above the free surface. The top, far side and bottom boundaries conditions were defined as free-slip walls while the hull was a no-slip wall. The upstream and downstream boundaries were pressure inlet and outlet respectively, defining known hydrostatic pressure values at the boundaries and with a prescribed inflow speed of  $U$ .

Table 2: Geometric characteristics of the CFD domain

Description	Symbol	Value	Unit
Basin width (half)	$W$	1.775	[m]
Basin depth	$d$	1.500	[m]
Water density	$\rho$	$9.983 \times 10^2$	[kg.m <sup>-3</sup> ]
Water dynamic viscosity	$\nu$	$1.028 \times 10^{-3}$	[kg.m <sup>-1</sup> .s <sup>-1</sup> ]

## 2.3 MESH MODEL

The computational domain was discretised using an unstructured hybrid tetrahedral mesh containing mainly tetrahedral cells. Hexahedron cells were used for the inflation layers around the body and the fluid free surfaces. This mesh was selected for the ability of tetrahedral cells to fit a relatively complex hull shape while easily accommodating future automatic remeshing process, and for the ability of the hexahedron cells to generate a smooth free-surface. The initial mesh model features the following parameters: the surface area of the mesh model of the BB2 hull was within 0.1% of the geometry model as defined by Overpelt et al. (2015), producing an accurate meshed hull form; a maximum mesh size of 1.562 m on the domain and  $1.12 \times 10^{-2}$  m on the hull with local refinement cells down to  $5.00 \times 10^{-4}$  m. An enhanced wall treatment function was used with a  $y^+$  of 50 for the inflation layer around the hull, casing and Aft Control Surfaces (ACS).

The total heights of the inflation layers was thicker than the boundary layer and the minimum total thickness matched 2 times the Prandtl's  $1/7^{\text{th}}$  power law theoretical estimate of turbulent boundary layer thickness over a flat plate (i.e.  $2 * 0.16 L_{pp} / Re_{L_{pp}}^{1/7}$ ) (White, 2002). A reduction of the  $y^+$  value towards a  $y^+$  of 1 was not deemed necessary given that minimal flow separation effect was anticipated to be relevant. An inflation layer was not created on the sail and its control surfaces as their viscosity in air has been deemed negligible and the UV remained surfaced at all times. This allows for an overall smaller mesh count compatible with smaller computing resources.

The boundary layer meshing methodology presented a significant difficulty regarding the boundary layer hull-free-surface interface. This is a unique issue due to the unconventional hull shape and the angle between the hull and the free surface. An alternative solution was utilized, consisting of the generation of a cubical subdomain around the UV hull as described in Figure 3. The inflation layer around the free surface stopped at the subdomain walls, and the inflation layer around the UV is then generated with no interruption from the free-surface inflation layer. Great care was taken to ensure the smallest space possible between the subdomain walls and the UV hull to limit the length of the free-surface on which no inflation layer was generated in the nearfield. This modelling method also simplified the remeshing process necessary to model the different heave and trim geometries. This mesh setup was thus used for the mesh independence study and the simulations proposed in this paper.

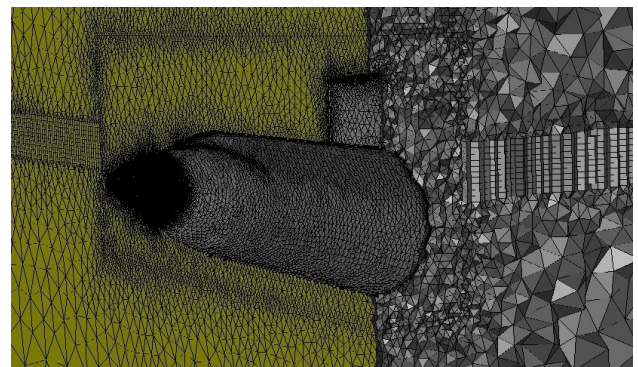


Figure 3: Section view on the longitudinal axis of the half-domain unstructured hybrid tetrahedral mesh with a rectangle subdomain around the UV hull. The free-surface inflation layer mesh stops at the subdomain external wall in all directions while the hull-casing-ACS inflation layer is complete.

## 2.4 MESH INDEPENDENCE STUDY

A mesh independence study was performed on the unstructured hybrid tetrahedral mesh described in Figure 3, using the UV hull surface mesh size as the refinement variable, and on the trimmed and heaved geometry corresponding to the highest Fr investigated.

Figure 4 presents the results of a Richardson extrapolation between 5 meshes of regularly decreased cell size with a total mesh cell count ranging from 6.3 to 11.3 million. The refinement step size was approximately  $\sqrt{2}$ . The changes in quantities over the grid refinement process are generally small which indicates a negligible effect of the mesh on the results. Moreover, at about 9.0 million cells, the drag predicted quantities were under 0.1% of discrepancy with the finest mesh investigated which corresponds to an acceptable threshold from which the results are deemed independent from the mesh influence. As a conservative measure, the 9.27 million elements mesh (half domain) was used in this study for the trimmed and heaved geometry corresponding to the highest Fr investigated (0.273). The cell count varies slightly between the different trimmed and heaved geometries used for the other values of Fr, and the cells count of the trimmed and heaved models used comprised between 9.26 and 9.37 million cells, while the zero heave and zero trim hull model had 9.09 million cells.

As a methodology check, a study of the free surface mesh size has also been carried out, confirming the mesh independence results and the validity of the method used. Figure 5 shows the drag for the different free surface cell sizes. The baseline free surface size ( $1.25 \times 10^{-2} \text{m}$ ) corresponds to the one that has been used for this study and is compared to a coarser ( $1.50 \times 10^{-2} \text{m}$ ) and a finer ( $1.00 \times 10^{-2} \text{m}$ ) mesh size. The 9.27 million elements mesh (half domain) presented above was used for the rest of the domain. The drag difference to the base resolution is 0.29 % for the coarser and 0.46 % for the finer mesh which is deemed negligible. Mesh refinement sizes applied are presented in Table 3 for clarity.

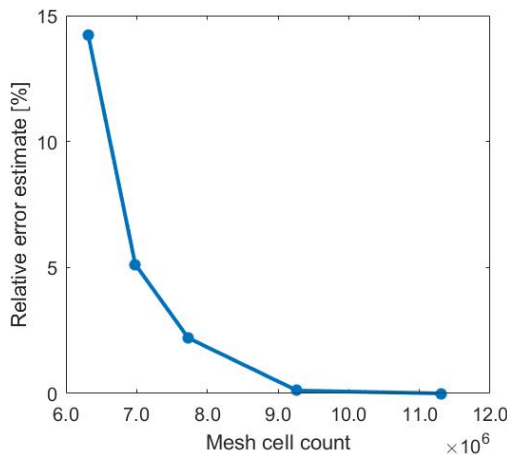


Figure 4: Relative error on the drag force for several mesh elements size from the finest 11.3 million cell mesh. Mesh cell count represents the half domain.

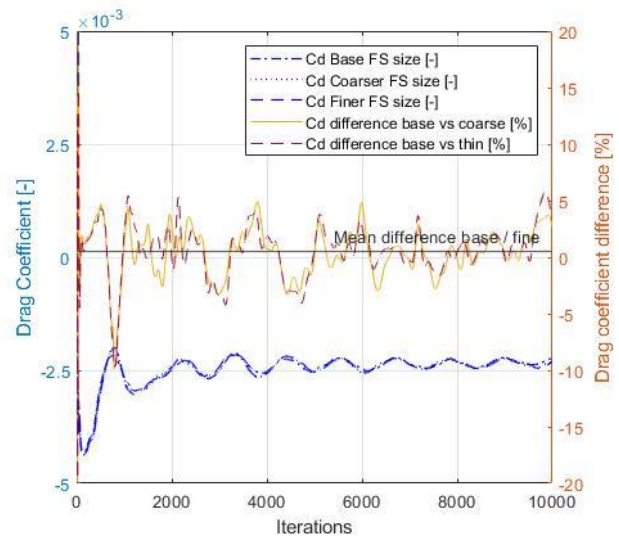


Figure 5: Drag coefficient difference for 3 free surface mesh size at Fr = 0.273 (1.12 m/s) over 10000 time iterations.

Table 3: Mesh refinement size (m) in use with the different free surface cell sizes tested.

Refinement location	Baseline free surface $1.25 \times 10^{-2}$ [m]	Coarse free surface $1.50 \times 10^{-2}$ [m]	Thin free surface $1.00 \times 10^{-2}$ [m]
Hull	$1.25 \times 10^{-2}$	$1.25 \times 10^{-2}$	$1.25 \times 10^{-2}$
Aft cone	$2.00 \times 10^{-3}$	$2.00 \times 10^{-3}$	$2.00 \times 10^{-3}$
Aft tip	$5.00 \times 10^{-4}$	$5.00 \times 10^{-4}$	$5.00 \times 10^{-4}$
ACS	$1.00 \times 10^{-3}$	$1.00 \times 10^{-3}$	$1.00 \times 10^{-3}$
BOI surface	$1.25 \times 10^{-2}$	$1.25 \times 10^{-2}$	$1.25 \times 10^{-2}$
BOI / Free surface edge	$5.00 \times 10^{-2}$	$5.00 \times 10^{-2}$	$5.00 \times 10^{-2}$

## 2.5 TRIM AND HEAVE MODEL VARIATION

The CFD model was set-up to match the experimental conditions. The experimental setup used a two-post mounting system with the forward post at the sail location, and the aft post on an additional vertical post as shown in Figure 6. This setup allows the physical model to move in 3 degrees of freedom (surge, heave and trim). The vertical displacements of the forward and aft posts were measured using LVDTs. The dynamic heave and trim of the model were calculated from the vertical displacement of the forward and aft posts. The experimental results showed that the dynamic positive (bow down) trim and negative heave (greater submergence) varied with constant forward speed. The positive trim and negative heave were found to be more important in magnitude when the forward speed was higher, as presented in Table 4. It is hypothesized that this is linked to the quantity of water runup at the UV bow. Since the CFD simulation was conducted with a single degree of freedom (surge) the numerical model was set up with the same constant heave and trim found from averaged results of the physical experiments. The heave and trim settings were different for each Fr investigated as

outlined in Table 4. A model with free heave and pitch (3 degrees of freedom) is out of the scope of this paper.

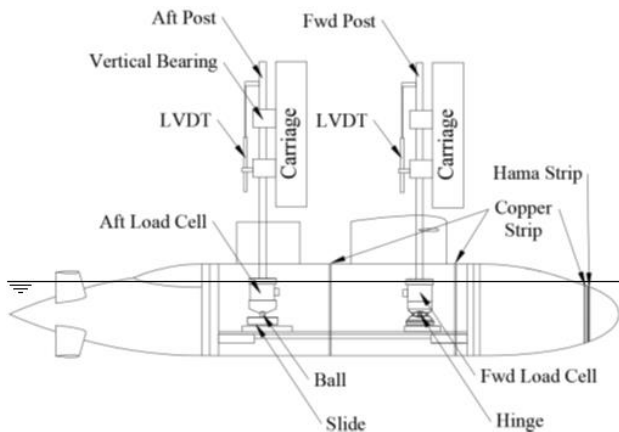


Figure 6: BB2 surfaced seakeeping model setup

Table 4: Vertical displacement and trim values at different Froude number values

Froude number [-]	Vertical displ. on aft post [mm]	Vertical displ. on forward post [mm]	Trim [deg]
0.117	-0.942	-1.757	0.109
0.156	-1.983	-3.929	0.261
0.195	-3.291	-7.161	0.519
0.234	-4.843	-12.223	0.990
0.273	-7.778	-19.533	1.577

Different numerical configurations were thus created to compare a horizontal hull (zero trim and zero heave) to the trimmed and heaved conditions corresponding to each speed investigated. The drag values were compared, and Figure 7 presents the results for the highest speed investigated over 10000 computing iterations. Results indicate that the drag difference is 7.5% on an average value from the 3000<sup>th</sup> step, hence is non-negligible. The 3000<sup>th</sup> step was selected as the bottom limit to compute the average as the simulation was not stable earlier. The images from CFD simulations in Figure 8 also show a significant change in the water runoff above the bow and fore part of the mid-body at a Fr of 0.273. The top picture represents the case with the UV model fixed at zero trim and heave. The bottom picture represents the case where the heave and trim were set to match the experiment, and the wave profile was found to be very similar to the experiment (see Figure 11).

Following these observations, several numerical configurations were then used to replicate the experimental heave and trim at the different speeds, requiring a new geometry configuration and a new mesh to be created for each Fr investigated. For example, the model is trimmed 1.577 degrees at a Fr of 0.273 to match the experiment, as shown in Figure 2.

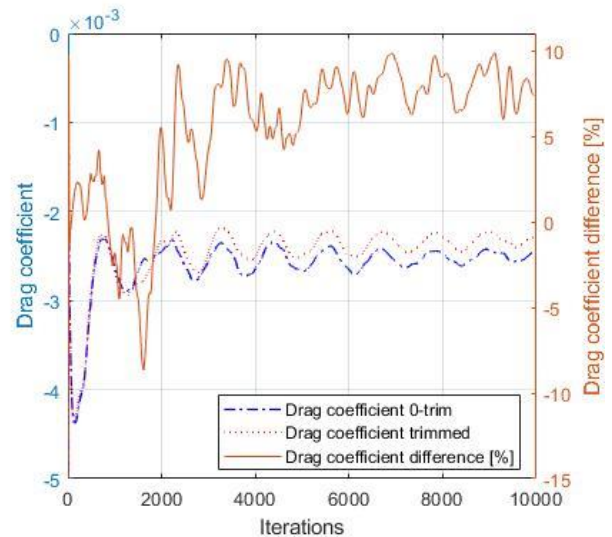


Figure 7: Drag coefficient [-] and drag coefficient difference [%] between the zero-trim and the trimmed and heaved surfaced BB2 over 10000 iterations (5ms) at a Froude number of 0.273.

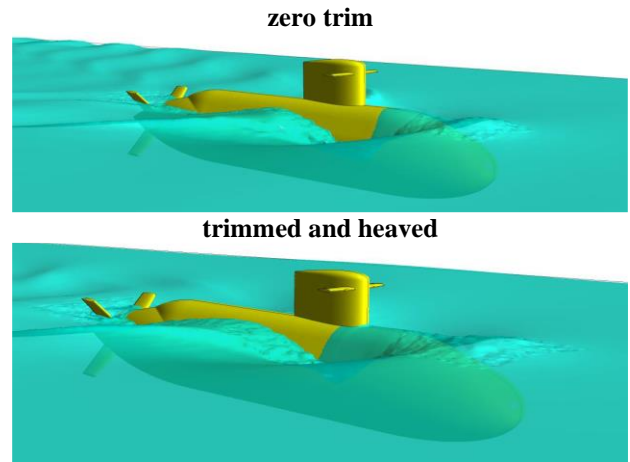


Figure 8: Wave profile over the surfaced BB2 hull for a horizontal setting (zero trim and zero heave) (top) and a trimmed and heaved geometry (bottom) at Fr 0.273.

## 2.6 ITERATION STUDY

Another challenging factor was determining the appropriate pseudo-time step to use. It was found at first that the simulation had unsteady drag results for pseudo-transient timesteps corresponding to a CFL condition of 1.0 and resulting in difficulties to converge with drag variations of around 15% above and under a mean value. This was especially visible for the lower Fr investigated as the drag force values are particularly small. Smaller values of timesteps were then selected, generating convergence issues on the overall simulations initially running for 5000 iterations. Therefore, the simulations ran for 10000 iterations with a pseudo-timestep of 5 ms which resulted in a CFL value less than 0.5. This provided stable results for the majority of required simulations. The simulations were running in approximately 15 hours with 120 cores synchronised at 3.4 GHz. The drag value results are shown

to be steady for the Fr values of 0.117 and 0.156 but present an unsteady behaviour for higher Fr that does not settle within the 10000 computing iterations as seen on Figure 10.

A case with 20000 computing iterations was investigated for the highest Fr, since it presented the larger amplitude oscillations, to assess if the unsteady convergence behaviour would disappear over longer simulations. Figure 11 shows that the oscillations are still visible for a prolonged run time, even though of slightly smaller magnitude. More pertinent, the comparison of the 10000 and 20000 iterations simulations showed that the mean drag coefficient difference over the last 2000 iterations was small: the mean drag coefficients were -0.0024 and -0.0023 for the 10000 and 20000 iterations simulations respectively, for the heaved and trimmed configuration; and the mean drag coefficient remained constant at -0.0025 for both simulations regarding the zero trim configuration. The difference in drag coefficient between the 2 configurations were 7.24 % for the 10000 iterations and 7.39 % for the 20000 iterations. This represents a discrepancy of 2.07 %, deemed small, and confirms that the shorter simulation is adequate for the presented results to be reliable. It is believed the unsteady behaviour at high Fr is a hydrodynamic phenomenon due to the fluctuations in the runup on the bow and the fore mid-body of the UV.

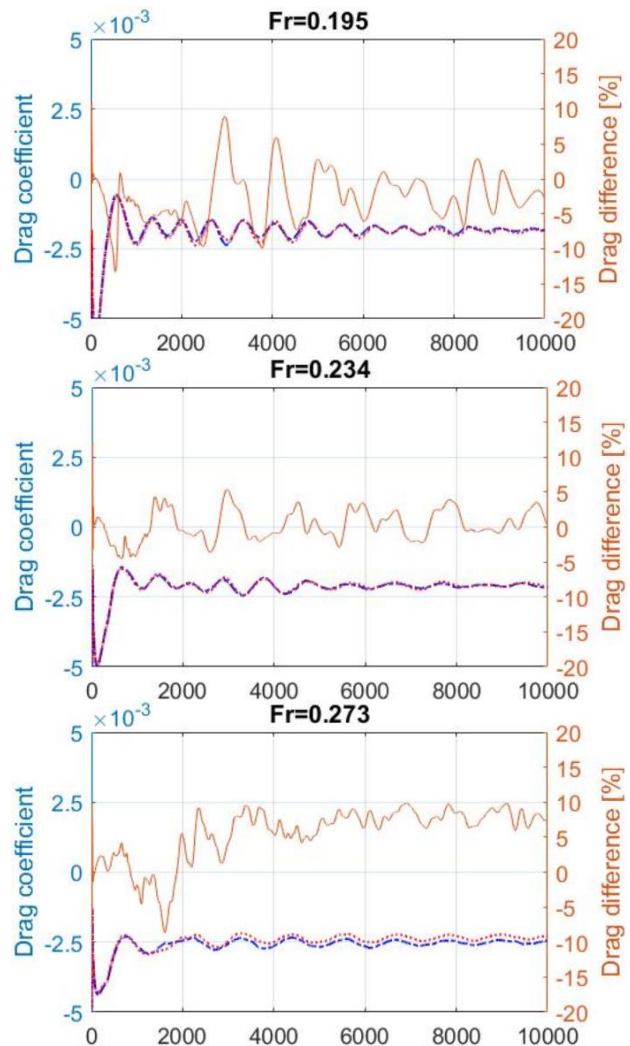
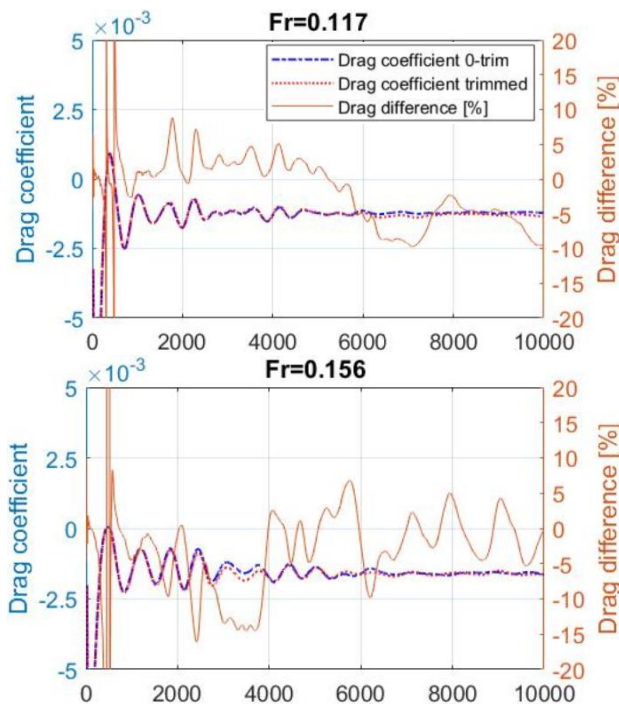


Figure 10: Drag coefficients between the 0-trim and the trimmed and heaved surfaced BB2 for Fr of 0.117 to 0.273 (5ms time iterations).

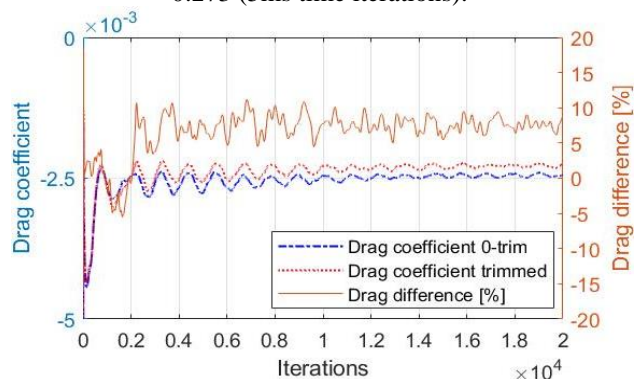


Figure 11: Drag coefficient between the zero heave and trim and the trimmed and heaved surfaced BB2 over 20000 computing iterations (5ms time iteration) for Fr of 0.273.

### 3. SURFACED UV IN CALM WATER

#### 3.1 DRAG VALIDATION AGAINST TOWING TANK EXPERIMENTAL DATA

Figure 12 shows the numerically predicted drag coefficient on the surfaced BB2 compared with the

experimental data as well as the difference between them. The results were averaged over 5700 iterations (5ms) from the 3000<sup>th</sup> iteration. The experimental uncertainty calculation was based on the ITTC method for resistance testing (ITTC, 2014) and included significant type A (repeatability and calibration of load cells) and type B (bias in the model displacement, towing speed and water temperature) uncertainties. The targeted uncertainty study was propagated for every Fr, and the maximum uncertainty in the experimental surge measurement at the 95% confidence level was  $\pm 3.05\%$ . The CFD uncertainty was calculated following ITTC (2017) method as demonstrated through the Richardson extrapolation, and the simulation numerical uncertainty was assessed at 0.16% of the drag coefficient, taken for the highest Fr to remain conservative. The maximum variation in speed between the experimental and the CFD values was 0.494% for the slowest speed investigated and presented a standard deviation of 0.1991. The experimental and numerical results and estimated uncertainties are presented in the Table 5.

A first observation is that the trend of the CFD results is in good agreement with the experiments. The average drag coefficient difference over the range of speeds investigated is 7.5 % and the maximum difference to the experimental data is 12.2 % at Fr of 0.156. These discrepancies are within the experimental uncertainty where available (for Fr of 0.117, 0.195 and 0.273) which coupled with the very good trend of the numerical values compared to the experimental data adequately validates this model for the surfaced fully appended BB2 simulations.

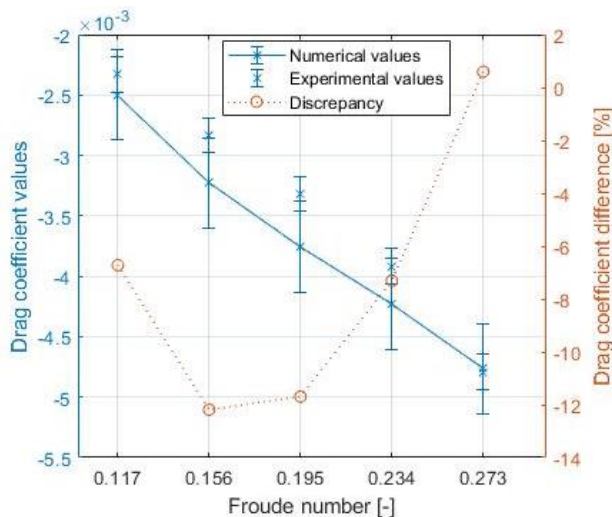


Figure 12: Numerical (trimmed and heaved) and experimental drag coefficient averaged values comparison for the range of speeds.

Table 5: Experimental and Numerical (trimmed and heaved) results and estimated uncertainties

Froude number [-]	Exp. Cd result	Estimated exp. uncertainty	Num. Cd result	Estimated num. uncertainty
0.117	-0.0023	-7.1075e <sup>-5</sup>	-0.0025	-4.0000e <sup>-6</sup>
0.156	-0.0028	-8.6433 e <sup>-5</sup>	-0.0032	-5.1200 e <sup>-6</sup>
0.195	-0.0033	-1.0121e <sup>-4</sup>	-0.0038	-6.0800 e <sup>-6</sup>
0.234	-0.0039	-1.1950 e <sup>-4</sup>	-0.0042	-6.7200 e <sup>-6</sup>
0.273	-0.0048	-1.4618e <sup>-4</sup>	-0.0048	-7.6800 e <sup>-6</sup>

### 3.2 FREE SURFACE PATTERN VALIDATION AGAINST TOWING TANK EXPERIMENTAL OBSERVATIONS

The last step of validation for the numerical model was to visually inspect and compare the predicted free surface pattern around the underwater vehicle. Due to the camera location in the model scale experiments it was not possible to closely inspect the free surface elevation in the ACS area. Hence, the comparisons are made around the bow and mid-body of the UV only. Comparison between the predicted free surface pattern and the physical experiment observations is shown for Fr = 0.273 in Figure 13. From the details presented in Figure 14 it is visible that the length of the water runup on the UV bow is very similar between the two pictures. A small ripple against the fore base of the sail, extending to approximately 1/4 of the sail length on its side is also visible on the CFD image and of realistic shape and position when compared to the picture from the experiment. The length of travel of the wave runup above the mid axis of the BB2 (up to the sail) was found to be similar for all Reynolds numbers from 0.117 to 0.273 experimentally, but the size (height) of the ripple significantly changed. The experimental picture resolution does not allow a more detailed quantification of this phenomenon at this stage. It is worth noting that the numerical model was not able to accurately predict this travel length of the water above the UV hull as depicted by Figure 13.

The overall numerical side wave profile was of realistic dimension, but the position of its trough is found to be much further forward in the numerical model than the experiment. The crest of this wave being approximately well positioned compared to the experimental picture means that the fore slope is the major difference. These observations are however indicative thus far. Further work is currently ongoing to experimentally measure the nearfield wave profile height distribution and to improve the prediction around these areas in order to quantify and understand the drag sensitivity to the phenomena.

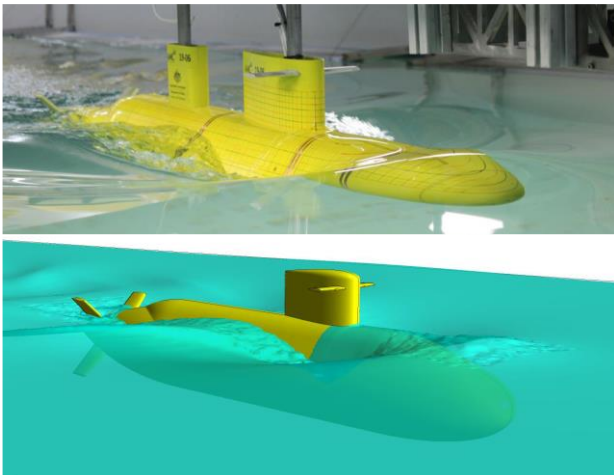


Figure 13: Experimental and numerical visualisation of the waves shape at  $Fr = 0.273$  in calm water.

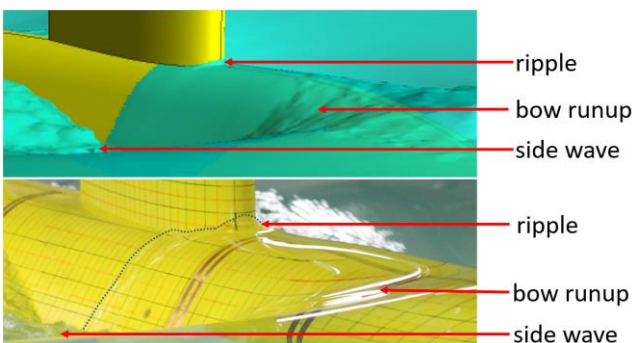


Figure 14: Detail of the free surface pattern and the runup toward the sail at constant  $Fr=0.273$  in calm water.

### 3.3 WAKE AND DRAG COEFFICIENT EVOLUTION AT SEVERAL SPEEDS

The evolution of the wave pattern is presented in Figure 15 which shows an isosurface of the water volume of fraction around the fully appended BB2 hull for the range of  $Fr$  investigated. Figure 16 details the water runup forming for the trimmed and heaved geometries, as per the observations from the experiments. It is visible that the bow wave travels further along the hull for greater speeds generating bigger side waves and also creating a small ripple at the base of the sail for the highest speed. Some wall effects are visible close to the hull side on the top view pictures and corresponds to the mesh subdomain wall position. It is visible that the bow wave travels further along the hull for greater speeds generating bigger side waves and also creating a small ripple at the base of the sail for the highest speed. At  $Fr$  of 0.234 and 0.273, reflection of the waveform on the side wall of the domain is observed. These observations are also to be expected in the experiment as the computational domain matched the towing tank.

Finally, Figure 17 presents the drag coefficient comparison between the horizontal ('zero trim') and the trimmed and heaved geometries (as per experiments). The results are also reported in Table 6. It can be seen that the numerical values are very close to the experimental ones, further confirming the validation of the model. The  $R^2$  of the numerical drag

coefficient is 0.994, hence close to a linear relationship and this does not allow for the identification of any wave interference effects on the drag at these speeds.

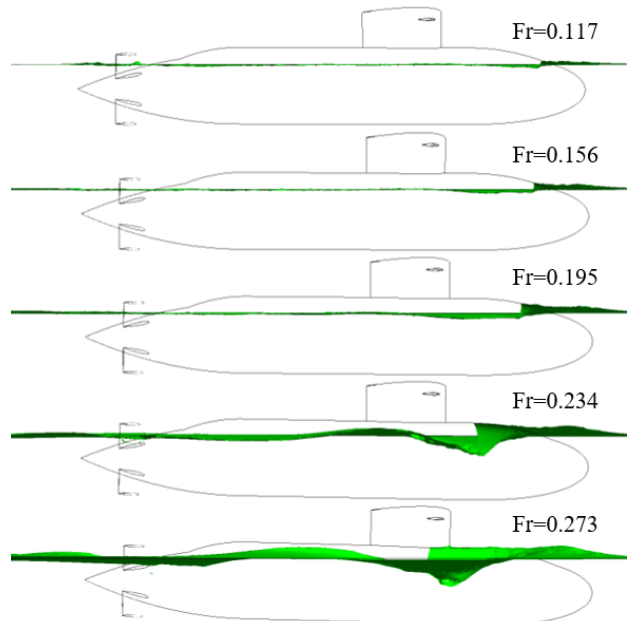


Figure 15: Evolution of the isosurface showing the volume fraction (0.5) over the BB2 surfaced hull for the Froude numbers investigated.

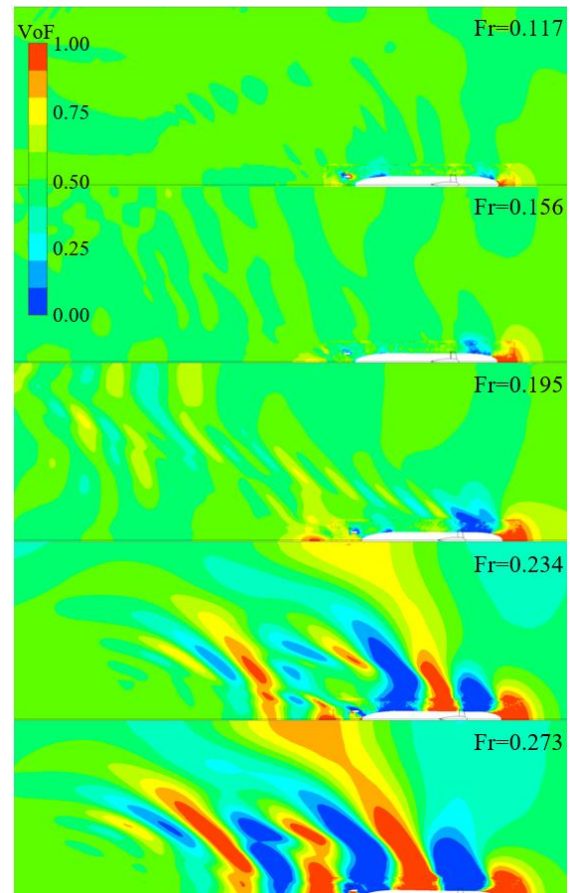


Figure 16: Half domain overview of the evolution of the volume fraction (0.5) over the buoyancy plane for the Froude numbers investigated.

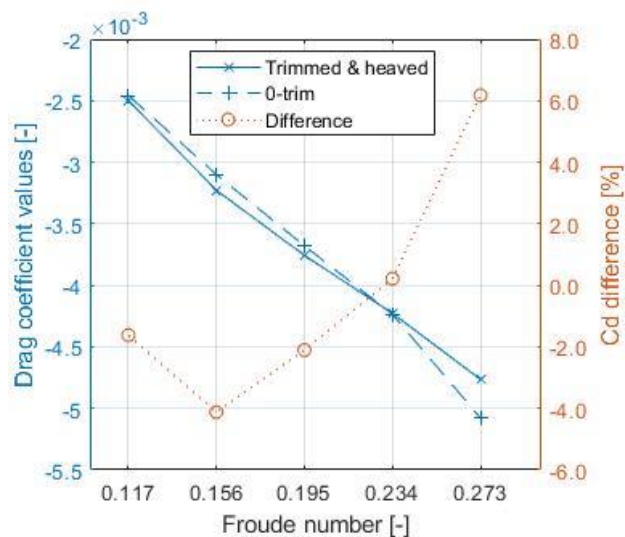


Figure 17: Drag coefficient variation comparison of CFD zero trim and trimmed geometries as a function of Froude number.

Table 6: Numerical drag coefficient values and comparison between configurations for each Fr number

Froude number [-]	Trimmed and Heave Cd	0-trim Cd	Cd difference [%]
0.117	-0.0025	-0.0025	-1.6227
0.156	-0.0032	-0.0031	-4.1214
0.195	-0.0038	-0.0037	-2.1060
0.234	-0.0042	-0.0042	0.2155
0.273	-0.0048	-0.0051	6.1749

#### 4. CONCLUSION

RANS-based CFD simulations were conducted for a fully appended surfaced BB2 model in a straight line manoeuvre and in calm water. The results allowed comparison between the numerical drag of the UV and experimental data in order to validate a surfaced appended UV CFD model.

The study included an investigation on the importance of modelling different trimmed and heaved geometries for each speed as it was found that the hull trims and sinks even in calm water. The drag difference was found to be significant between a horizontal hull and a trimmed-heaved hull at the same speed.

The numerical model was developed using a hybrid tetrahedral mesh with a rectangle subdomain around the hull to assist in the generation of clean and continuous inflation layers around the submerged hull and the free surface. The volume of fraction representing the free surface elevation was then plotted, giving insight into the inception and development of the waves around the surfaced UV hull for the different speeds investigated.

The meshing methodology used gave good results, with a high-fidelity trend in the drag values changes over the speed range and drag differences between the numerical and experimental values were within the experimental uncertainty. It is expected that a full inflation layer of the free surface that extends to the hull surface would help reduce this drag difference as well as provide a better description of the wave formation in proximity of the hull.

It was observed that for the higher speeds (for which the trim angle and submergence is greater than at slower speeds), the drag difference between a zero trim and a heaved and trimmed configuration is not necessarily more important than for slower travelling motion but is more stable as shown by Figure 10. It can be hypothesized that higher speed runs are less sensitive to the towing tank carriage motion irregularities, probably because the amount of water above the hull's bow act as a damping mechanism.

Finally, a visual comparison of the shape and position of vessel induced waves was conducted between the numerical simulations and some experimental pictures. This confirmed that the CFD model was able to replicate the bow water runup observed. However, it failed to fully capture the side wave shape.

To date, the ability of the model to accurately predict the drag to the forward motion of a surfaced fully appended UV has been demonstrated. This study is a significant first step in the development of a more comprehensive model allowing movements in 3 degrees of freedom, hence allowing investigations of the heave and trim motion coupling of a surfaced UV in waves. Further work is currently ongoing to experimentally measure the nearfield wave profile height distribution and to improve the prediction of the model around these areas to better understand the wave distribution around a surfaced UV and its coupled effect with drag.

#### 5. ACKNOWLEDGMENTS

The authors acknowledge the support of Thomas McLean and Julia Blackman in providing the experimental dataset used as validation, as well as the Defence Science and Technology Group (DST) of the Australian government for the funding and guidance of their research project.

#### 6. REFERENCES

1. ALVAREZ, A., BERTRAM, V. and GUALDESI, L. (2009) *Hull Hydrodynamic Optimization of Autonomous Underwater Vehicles Operating at Snorkeling Depth*, in: *Ocean Engineering*, 36(1), pp. 105–112. doi: 10.1016/j.oceaneng.2008.08.006.
2. BHATTACHARYYA, R. (1978) *Dynamics of marine vehicles*. New York: John Wiley & Sons Inc. 978-0-471-07206-5

3. BLACKMAN, J. (2019) *Investigation into the Heave and Pitch Motions of a Surfaced Submarine in Head Seas*. BEng (Hons) Thesis, University of Tasmania - Australian Maritime College, Launceston.
4. BOVIS, A. (2017) *Hydrodynamique navale: Le sous-marin*. 2nd edn, Presses de l'ENSTA, Palaiseau. 978-2-7225-0953-5
5. CHUN, H. H. (1992) 'On the Added Resistance of SWATH Ships in Waves', *Transactions of the Society of Naval Architects of Korea*, 29(4). doi: 10.1111/j.1365-246X.1972.tb05820.x
6. DAUM, S., GREVE, M. and SKEJIC, R. (2017) *On the Added Resistance of Underwater Vehicles in close Proximity to Regular Waves*, in. Warship 2017: Naval Submarines & UUVs, Bath, UK, June 14-15
7. DOUTRELEAU, Y., LAURENS, J.-M. and JODET, L. (2011) *Résistance & Propulsion du Navire Résistance à l'Avancement Helice Appareil Propulsif Niveau C*, Ellipses Marketing, Paris. 978-2-7298-6490-3
8. GATES, P. J. and LYNN, N. M. (1990) *Ships, submarines, and the sea*. London; Washington; Sydney: Brassey's (Sea Power - Naval Vessels, Weapons Systems and Technology Series). 978-0-08-034735-6
9. HERMANSKI, G. and KIM, S. (2010) *Surface Seakeeping Experiments with a Model of a Submarine*, in. 11th International Symposium of Practical Design of Ships and Other Floating Structures: 2010 PRADS, Rio de Janeiro, Brazil, September 19-24: NRC Publications Record.
10. HUONG, Y. T. (2018) *Numerical Analysis on the Effect of Submergence Depth on the Barehull Model Scaled BB2 at AMC Towing Tank*. BEng (Hons) Thesis, University of Tasmania - Australian Maritime College, Launceston.
11. ITTC (2011) *Practical Guidelines for Ship CFD Application*. Recommended Procedures and Guidelines 7.5-03-02-03.
12. ITTC (2014) *Guide to the Expression of Uncertainty in Experimental Hydrodynamics*. Recommended Procedures and Guidelines 7.5-02-01-01.
13. ITTC (2017) *Uncertainty Analysis in CFD Verification and Validation, Methodology and Procedures*. 7.5-03-01-01.
14. KUMAR, C. S. *et al.* (2018) *Boundary layer tripping study on a Generic Submarine Model in Water*, in. 21<sup>st</sup> Australasian Fluid Mechanics Conference, Adelaide, Australia, December 10-13.
15. LEONG, Z. Q. *et al.* (2015) *Rans-based CFD prediction of the hydrodynamic coefficients of DARPA SUBOFF geometry in straight-line and rotating arm manoeuvres*, in. Transactions of the Royal Institution on Naval Architects - Part A: International Journal of Maritime Engineering, 157, pp. A41-A51. doi: 10.3940/rina.ijme.2015.al.308.
16. LEWIS, E. V. (ed.) (1988a) *Principles of Naval Architecture*. Jersey City: Society of Naval Architects & Marine Engineers. 978-0939773015
17. MCLEAN (2019) *An Investigation into the Resistance of a Surfaced Submarine*, BEng (Hons) Thesis, University of Tasmania - Australian Maritime College, Launceston.
18. OVERPELT, B., NIENHUIS, B. and ANDERSON, B. (2015) *Free Running Manoeuvring Model Tests On A Modern Generic SSK Class Submarine (BB2)*, in. PACIFIC International Maritime Conference, Sydney, Australia, October 6-8.
19. RENILSON, M. (2018) *Submarine Hydrodynamics*. Softcover reprint of the original 2nd ed. 2018 edition. Cham, SWITZERLAND: Springer. 978-3-319-16184-6
20. WHITE, F. M. (2002) *Fluid Mechanics*. 5th Edition. Boston: McGraw-Hill. 978-0-07-240217-9